Spatial Information Research
https://doi.org/10.1007/s41324-024-00582-0

Estimating above-ground biomass of trees outside forests using multi-frequency SAR data in the semi-arid regional landscape of southern India

A. S. Anjitha[1] · C. Sudhakar Reddy[2] · N. Nitish Sri Surya[2] · K. V. Satish[2] · Smitha V. Asok[1]

Received: 10 February 2024 / Revised: 6 April 2024 / Accepted: 8 April 2024

Abstract
Trees outside forests are vital for sustainable resource management and play a crucial role in the sequestration of carbon. This study attempted to estimate the above ground biomass (AGB) of trees outside forests utilizing the datasets of ALOS PALSAR-2 (L-band) and Sentinel-1 (C-band), with a focus on a semi-arid region in Sri Sathya Sai district of Andhra Pradesh, India. Here, we employed random forest (RF) algorithm integrating AGB observed over a large-scale ecological plot and remote sensing technology for generating 3 models (Model-1 (M1), Model-2 (M2), and Model-3 (M3)). Backscattering coefficients (VV and VH) and H-α dual pol decomposition parameter, anisotropy (A) from Sentinel-1 were applied for M1, and the backscattering coefficients (HV and HH) and the band ratio (HV/HH) from ALOS PALSAR-2 data were utilized in M2. M3 is the ensemble of parameters from both sensors. Validating the three models found that the R^2 values fall between 0.44 and 0.64, the RMSE between 1.89 t/ha and 2.49 t/ha, and the MAE between 1.56 t/ha and 1.99 t/ha. The results of the study suggest that both Sentinel-1 and ALOS PALSAR-2 data can be employed for AGB estimation in semi-arid regions incorporating machine learning algorithms like RF. The results of the study are crucial for sustainable land management and reducing uncertainty using data from large-area ecological plot and multi-frequency synthetic aperture radar (SAR).

Keywords Above ground biomass · Random forest · Sentinel-1 · ALOS PALSAR · Synthetic aperture radar · Trees · Semi-arid

1 Introduction

Trees outside forests play a crucial role in sustainable natural resource management by providing a variety of goods, including timber, fruits, fodder, and offering essential ecosystem services like water, carbon, and biodiversity. Biomass serves as a responsive indicator of changes in the environment and the operational dynamics of ecosystems. Quantifying the biomass of vegetation at the regional scale adds to the monitoring and understanding of ecological functioning within the area [1]. AGB is one among the essential climatic variables as well as a potential essential biodiversity variable for understanding the ecosystem structure and function [2]. Vegetation and biomass are the significant factors affecting not only biodiversity and environmental processes, but also ecosystem variability and perseverance, which indicates the need for monitoring and maintaining community biomass [3]. In addition, biomass measurement encourages identifying and monitoring the areas at risk of degradation and desertification, particularly in the semi-arid and arid regions, for sustainable management of land use [4].

Destructive sampling techniques used in traditional biomass assessment methodologies are not feasible, as they are expensive and time consuming, particularly in vast areas [5, 6]. The use of remote sensing technology made possible a cost-effective method for spatially explicit monitoring of

✉ C. Sudhakar Reddy
drsudhakarreddy@gmail.com

[1] Department of Environmental Sciences, All Saints' College, Thiruvananthapuram, Kerala 695007, India

[2] Forest Bioaffiliationersity and Ecology Division, National Remote Sensing Centre, Indian Space Research Organisation, Balanagar, Hyderabad, Telangana 500037, India

Published online: 15 May 2024

vegetation biomass and disturbances [3, 7]. Studies on AGB estimation have been conducted with data obtained from different sensors, including optical, microwave, LiDAR, and hyperspectral remote sensing. By taking into consideration the optical data, the major drawback in AGB estimation is that it gets saturated due to the less sensitivity to biomass, especially in high biomass regions [5, 8–10]. The high cost of acquisition and non-availability of space-borne LiDAR data obstacles to LiDAR based AGB estimation.

The advantage of SAR data is that it can operate in all weather, day and night [8] and it can penetrate clouds and tree canopy, and exhibit a volume scattering mechanism [11, 12]. The different wavelengths (X, C, S, L, P), polarizations (HH, VV, HV, VH) and incident angles in SAR data influence the backscattering coefficient, which in turn shows varied sensitivity to AGB. The frequency of the SAR signal determines the length of penetration into the vegetation canopy at specific incident angles [11–13]. Due to the higher penetration potential and sensitivity to tree trunk of L-band data, it is being extensively investigated to increase the accuracy of AGB estimate [8, 14–20]. The Japan Aerospace Exploration Agency (JAXA) made ALOS PALSAR-2 ScanSAR data with a spatial resolution of 25 m freely accessible, and it is among the most extensively utilized sensors for estimation of biomass globally. Vegetation biophysical parameters are more effectively retrieved by utilizing longer wavelengths along with cross-polarized (VH or HV) data, as opposed to shorter wavelengths combined with co-polarized (VV and HH) data. This superiority is attributed to the depolarization of the incoming signal that occurs due to multiple scatterings within the vegetation volume [13]. Otukei and Emanuel, 2015 used backscattering coefficients for HV and HH polarizations of ALOS PALSAR to estimate the AGB of Bwindi Impenetrable National Park (BINP) in the south-western part of Uganda [8]. A model based on bagging stochastic gradient boosting (BagSGB) was employed by Carreiras et al., 2013 for the estimation of AGB in Miombo savanna woodlands of Mozambique in East Africa with the backscatter intensity from ALOS PALSAR data, obtaining a correlation coefficient of 0.95 [15]. Chang et al., 2022, in their study, found the significance of ALOS PALSAR L-band data in mapping the tundra shrub leaf area index and biomass as well [21].

Though the C-band cannot penetrate deep into the canopy [6, 22], it can penetrate through foliage and get subsequently scattered by the trunk and primary branches of trees [10]. The potential of the C-band in estimating biomass has been proven by various investigators, singularly or in combination [6, 10, 23–25]. Sentinel-1 in combination with Worldview-3 was used for the vegetation mine rehabilitation area by Bao et al., 2019, yielding an accuracy of $R^2 = 0.79$ [24]. Roy et al., 2021, predicted the biomass and tree density of *Shorea robusta* dominated forest cover using Sentinel-1 backscattering coefficients and Sentinel-2 derived EVI with a R^2 of 0.45 and 0.87 for biomass and tree density estimation, respectively [10]. Sentinel-1 coherence was utilized for AGB estimation by Cartus et al., 2022, in a semi-arid forest in California [25].

In addition, the incorporation of polarimetric decomposition parameters from Sentinel-1 data was found to have sensitivity towards the vegetation biophysical characteristics as well. The polarimetric decomposition technique was originally developed for quad-polarized data and later modified for dual-polarized data like those from Sentinel-1 [26]. In crop monitoring, Dave et al., 2023 found an increase in R^2 values through the incorporation of decomposition parameters [26]. De Petris et al., 2021 found the feasibility of decomposition parameters from Sentinel-1 in mapping the damaged apple orchards in Italy [27]. Furthermore, the alpha angle and entropy generated from Sentinel-1 dual polarimetric decomposition were utilized by Jesus et al., 2023 for the estimation of the AGB of arboreal Caatinga [28]. However, the polarimetric decomposition of Sentinel-1 dual-polarized data is rarely employed in the context of estimating vegetation biomass.

Over the above, several investigators have illustrated the utility of integrating different SAR bands in retrieving vegetation biophysical parameters [29, 30]. For instance, Velasco Pereira et al., 2023 investigated the changes in biomass in Mediterranean pine forests through random forest and yielded a highest performance from the fusion of Sentinel-1, ALOS PALSAR-2, and Landsat 8 data [22]. An integration of L-band ALOS PALSAR, C-band RADARSAT-2, and X-band TerraSAR-X, datasets gave improved results for quantifying AGB ($R^2 = 0.83$), canopy cover ($R^2 = 0.83$) and total canopy volume ($R^2 = 0.85$) in the African savannas by Naidoo et al., 2015 [31]. The machine learning regression approach has gained popularity in AGB estimation over the past several years, even though no single technique has shown to be the best for predicting AGB in selected geographic region [32, 33]. Owing to the relative ease of tuning and the robustness found in previous studies in prediction of AGB [6, 34–37], random forest algorithm was selected for the present study.

Numerous studies have considered the potential of radar data in AGB estimation, showing excellent agreement with the vegetation biophysical parameters. Most of the studies are focused on forest ecosystems. Less attention is given to the biomass contributed by the arid and semi-arid ecosystems to the total terrestrial ecosystem. However, only a limited number of studies have been done at the local level for the trees outside the forest with the actual biomass of the selected region so far. Due to the heterogeneous distribution and variation in vegetation density, AGB estimation in

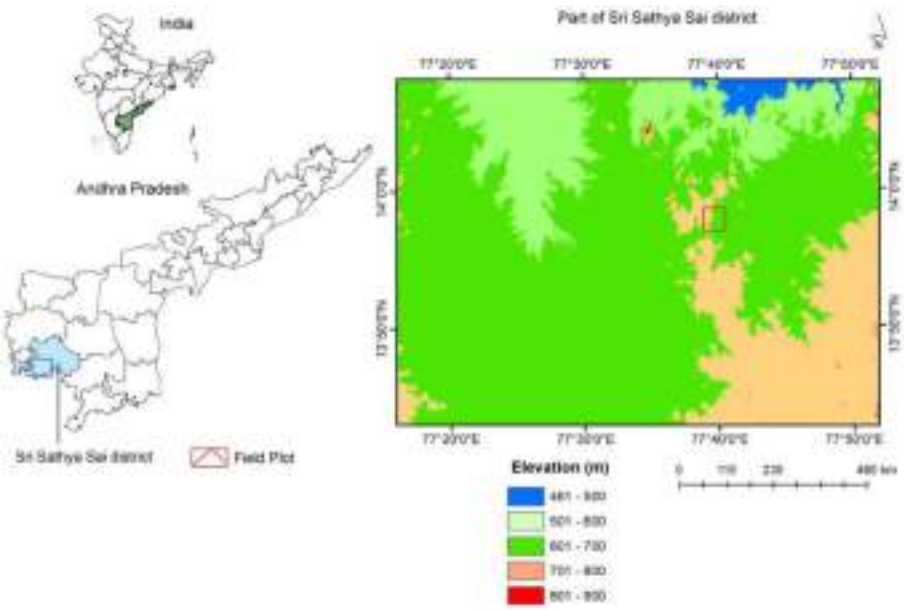

Fig. 1 Study area showing distribution of elevational gradient

a semi-arid zone is challenging. In the present study, we utilized multi-frequency data from Sentinel-1 and ALOS PALSAR-2 sensors for quantifying AGB in a semi-arid region of India. The quantitative assessment of vegetation biomass in semi-arid regions is a key source for assisting sustainable land management of the area and will help to identify the most vulnerable regions to the changing climate scenario.

The primary objectives of the study were to estimate the vegetation AGB in a semi-arid environment utilizing the random forest algorithm, and to evaluate the potential of Sentinel-1 and ALOS PALSAR-2 SAR sensors operating at C and L-bands, respectively.

2 Methodology

2.1 Study area

We selected a 2587 km^2 area in the semi-arid region of the Sri Sathya Sai district of Andhra Pradesh for the present study, which is coming under the "Deccan Plateau" phytogeographic zone in southern India. A variety of habitat types occupy this region, including scrublands, grasslands, orchards, long fallow, stony lands, built-up areas, seasonal streams, and remnants of dry deciduous and dry evergreen scrub vegetation as well. The region experiences hot, dry weather for most of the year, with a yearly average temperature of around 25.8 °C. The annual precipitation received is 620 mm, with September experiencing the peak at 161.2 mm [38]. The area had patches of trees and scattered individual trees as well. The major tree species found in the region are *Tamarindus indica* L., *Mangifera indica* L., *Ficus religiosa* L., *Pongamia pinnata* (L.) Pierre, *Grevillea robusta* A.Cunn. ex R.Br., *Azadirachta indica* A.Juss., and *Wrightia tinctoria* (Roxb.) R.Br. There are two palm species commonly found in the study area are *Cocos nucifera* L. (cultivated) and *Phoenix sylvestris* (L.) Roxb. (wild). Dense patches of the invasive woody species - *Prosopis juliflora* (Sw.) Raf. were also present [38]. Fig. 1 shows the study area selected for the current study. Vegetation types present in the study area are shown in Figs. 2, 3 and 4.

Fig. 2 *Pongamia-Wrightia-Azadirachta* tree community in Palasamudram

2.2 Field AGB calculation

The study has used a field inventory dataset of 900 ha large area plot, which was chosen to represent the geographical variation of this semi-arid region [38]. The sampled area covers 0.35% of the regional landscape. The percentage area

Fig. 3 Linear stratum of trees outside forests representing *Tamarindus indica*

Fig. 4 Mixed scrub and dry grassland

sampled for vegetated landscape is 0.70%. The methodology adopted for the study is given in Fig. 5. The diameter at breast height and height for individual trees were measured. Then the pan-tropical equation suitable for multiple species proposed by Chave et al., 2014 (Eq. 1) was used to calculate the plot level AGB [39].

$$AGB = 0.0673 * (\rho * D^2 * H)^{0.976} \quad (1)$$

where AGB is above ground biomass in kg, ρ is specific wood density in g/cm3, D is diameter at breast height (DBH) in m, and H is height in m.

2.3 Remote sensing data processing

2.3.1 ALOS PALSAR-2 data

We acquired ScanSAR L-band data of ALOS-2 PALSAR-2 (Level 2.2) having a spatial resolution of 25 m for the month of December, 2022 through Google Earth Engine (GEE) [56] [https://code.earthengine.google.com/]. The level 2.2 data are preprocessed for radiometric and topographic corrections. The data has acquisition in HH and HV polarizations in 16-bit digital levels (DN). Backscattering coefficient gamma naught values in decibel units were generated from the DN values for each polarization using Eq. 2. and the ratio band (HV/HH) was generated from the linear HV and HH bands using the 'terra' package in R-4.3.0 [57, 58] [https://cran.r-project.org/package=terra].

$$\gamma 0 = 10 * \log_{10}(DN^2) - 83.0\ dB \quad (2)$$

2.3.2 Sentinel-1 data

Single look complex (SLC) image data of the European Space Agency's (ESA) Sentinel-1 mission was acquired from the Copernicus Open Access Hub [59] [https://dataspace.copernicus.eu/], for the same month (December, 2022) as that of ALOS PALSAR-2 data in the interferometric wide swath (IW) mode. The dataset was dual-polarized with VH and VV bands. The pre-processing of Sentinel-1 was done using SNAP version 8.0 software [60] [https://step.esa.int/main/download/snap-download/], involving subsetting, calibration, multi-looking, speckle filtering, and terrain correction. Speckle noise was reduced using the refined Lee filter with a 7×7 window size. Range Doppler terrain correction using SRTM 1 s HGT DEM is performed for removing surface roughness, and pixel values were converted to back scattering coefficients in decibels through radiometric calibration for both polarizations.

2.3.2.1 H-α dual pol decomposition SAR data can be categorized according to its scattering mechanism through polarimetric decomposition. H-α dual pol decomposition, an incoherent decomposition technique based on eigenvector and eigenvalue, is a modified version of Cloude and Pottier decomposition [26, 40]. Polarimetric decomposition of Sentinel-1 involves the generation of scattering matrix, generation of the coherency matrix and then the decomposition parameters alpha angle (α), anisotropy (A), and entropy (H), are determined by using the eigenvalues and eigenvectors of the coherency matrix [T] [26, 41]. H ranges from 0 to 1, defining the degree of scatter randomness. It is proportional to the degree of depolarization and the number of dominating scattering processes [27] and is given as Eq. 3.

$$\mathrm{H} = \sum_{\mathrm{i}=1}^{2} (-\mathrm{P_i log_2 P_i}) \quad (3)$$

where

$$P_i = \frac{\lambda_i}{\sum_{j=1}^{2} \lambda_j}$$

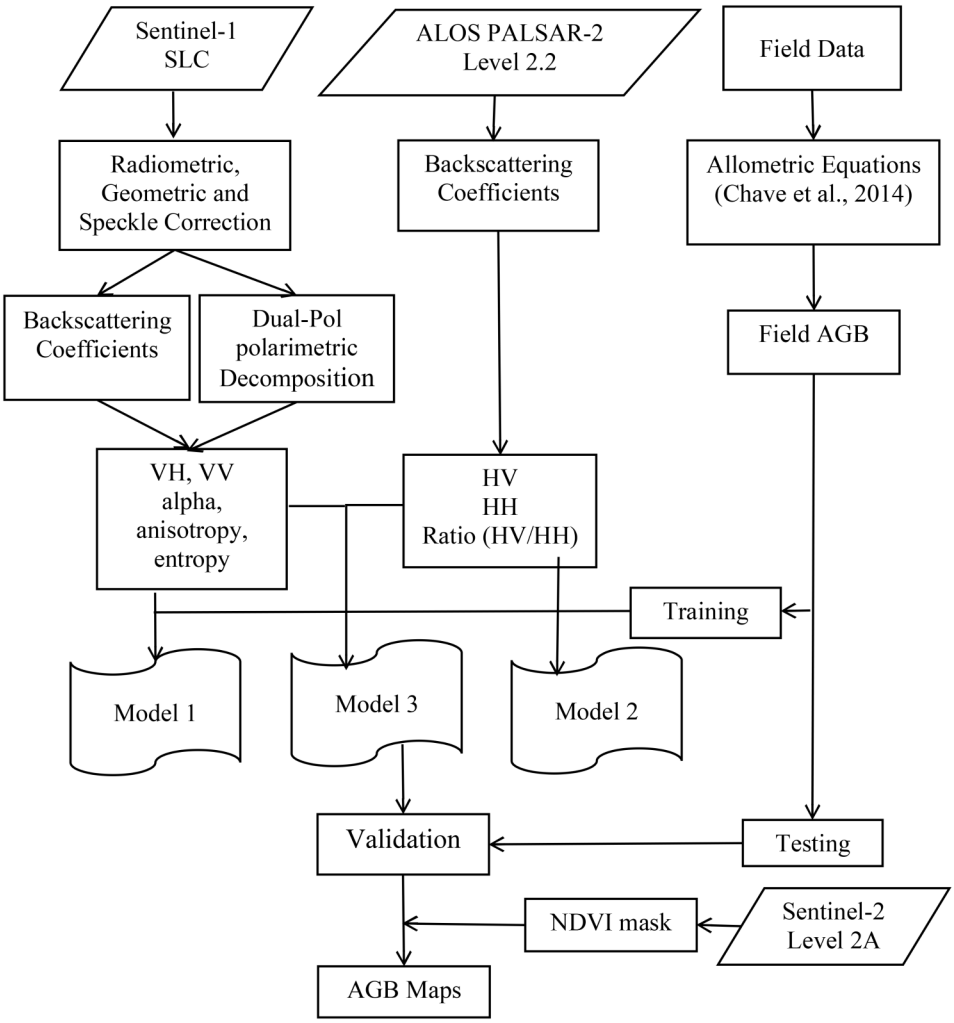

Fig. 5 Workflow of the methodology adopted

and λ is the local eigenvalue. In terms of the variations in scattering mechanisms, anisotropy (A) offers further details regarding H, quantifying the difference in strength between the primary and secondary scattering mechanisms, which is correlated with the degree of polarization of the signal [27]. A is calculated as Eq. 4:

$$A = \frac{\lambda_1 - \lambda_2}{\lambda_1 + \lambda_2} \tag{4}$$

Again, the α parameter can be used to identify the different scattering mechanisms like volume, double-bounce, and surface scattering. It can be computed using the Eq. 5.

$$\alpha = \sum_{i=1}^{2} P_i \alpha_i \tag{5}$$

where

$$\alpha_i = \cos^{-1}\left(\frac{|\lambda_1 + \lambda_2|}{\sqrt{2}\sqrt{|\lambda_1|^2 + |\lambda_2|^2}}\right)$$

All the raster layers generated were resampled to 100 m grid size through the bilinear interpolation approach.

2.3.3 Sentinel-2

The cloud free Sentinel-2 Level 2 A product acquired on 17th February 2023 was downloaded for calculating the most widely utilized vegetation index, Normalized Difference Vegetation Index (NDVI). NDVI was calculated in ArcMap 10.8 software for masking out non-vegetated areas, including water bodies and barren lands. NDVI quantifies the vegetation by evaluating the difference between the two spectral bands of the photosynthetic output, NIR and red bands. NDVI is a standardized way to measure the healthy vegetation whose value falls between − 1 and + 1, where the higher value indicating healthy or dense vegetation and the

lower value indicating less or no vegetation [42]. NDVI was calculated using Eq. 6. and the areas where the NDVI values were less than 0.2 were masked out to get the vegetation cover of the study area.

$$\mathrm{NDVI} = \frac{\mathrm{NIR} - \mathrm{Red}}{\mathrm{NIR} + \mathrm{Red}} \tag{6}$$

2.4 Statistical analysis

A total of 8 variables were derived from the radar data, which includes the backscattering coefficients for HV and HH polarizations and the ratio band (HV/HH) from ALOS PALSAR-2, the backscattering coefficients for VH and VV polarizations, and the polarimetric decomposition parameters alpha angle (α), anisotropy (A), and entropy (H). The degree to which field-observed AGB and the remote sensing variables are related was analyzed for the field calculated AGB values by Pearson correlation analysis. Further multicollinearity analysis was done before generating the models. Multicollinearity is a state where the predictors in a regression model are linearly dependent. The polarimetric decomposition parameters, entrtropy and alpha, were removed due to multicollinearity.

2.5 Random forest (RF) modeling

Random Forest (RF), a powerful machine learning algorithm, was put forwarded by Breiman Leo in 2001, and is mainly used for regression, classification, and survival analysis [43]. The bagging algorithm is utilized in RF to partition the training datasets into bootstrap datasets, which are sub-training datasets. The bootstrap datasets typically contain two-thirds of the whole samples from the training datasets; these datasets are referred to as "in-bag" data since they are used to test the RF model, and the remaining data is referred to as "out-of-bag" data [5, 34].

Three models were developed with individual sensor data and their combinations using the RF algorithm using the 'randomForest' package in R-4.3.0 [61] [https://cran.r-project.org/package=randomForest], where field observed AGB was taken as the dependent variable and parameters from remote sensing as the independent variables.

Three prediction models, Model-1 (M1), Model-2 (M2), and Model-3 (M3), were generated using the RF algorithm for each individual sensor and in combination of both sensors with the test data. The model generated with Sentinel 1 data, M1, gamma naught for VV and VH polarizations, along with the polarimetric decomposition parameter anisotropy (A), was used. For ALOS PALSAR based model, M2, the backscattering coefficient gamma naught for both HH and HV polarizations and the band ratio (HH/HV) were used as the variables. Further, the variables from both sensors were combined for developing the third model (M3).

2.6 Model evaluation and assessment

Only the 1 ha plots where the number of trees was greater than 10 were considered in building the model and accuracy assessment. Considering the plots with less number of trees could possibly reduce the prediction accuracy as the signal strength will be insignificant. Additionally, to avoid the model overfitting, the data was split into testing and training datasets after the outliers were removed. 80% of the data was utilized as the training dataset, while the remaining 20% was used for testing. Three indices were calculated for accuracy assessment, such as the coefficient of determination ($R^{2)}$, mean absolute error (MAE), and root mean square error (RMSE), and values were compared for the models. The value of R^2 spans from 0 to 1, with the values closer to one indicating the best fit of the model. The discrepancy between the actual and anticipated values is measured by the RMSE value. The model fits the data better when the RMSE and MAE values are lower. The metrics' calculation equations are given as:

$$R^2 = 1 - \frac{\sum_{i=1}^{n}(y_i - \widehat{y}_i)^2}{\sum_{i=1}^{n}\left(y_i - \bar{y}_i\right)^2}$$

$$\mathrm{RMSE} = \sqrt{\sum_{\mathrm{i}=1}^{\mathrm{n}} \frac{(\widehat{\mathrm{y}}_\mathrm{i} - \mathrm{y}_\mathrm{i})^2}{\mathrm{N}}}$$

$$\mathrm{MAE} = \frac{1}{\mathrm{N}} \sum_{\mathrm{i}=1}^{\mathrm{n}} |\widehat{\mathrm{y}}_\mathrm{i} - \mathrm{y}_\mathrm{i}|$$

where, $\mathrm{y_i}$ and $\widehat{y_i}$ are the observed and predicted AGB, respectively, $\bar{y}_i$ is the mean of observed AGB, and N is the number of data used for evaluation.

3 Results

A total of 2884 trees were found in the 900-ha area with 314 sampling plots, where the number of trees ranged from 1 to 185 in individual plots. The number of 1 ha plots with trees more than 10 was 67. The plot level in situ AGB varied between 0.01 t/ha and 45.86 t/ha, among which only 8 plots were having AGB greater than 10t/ha. The boxplot of field assessed AGB is given in Fig. 6.

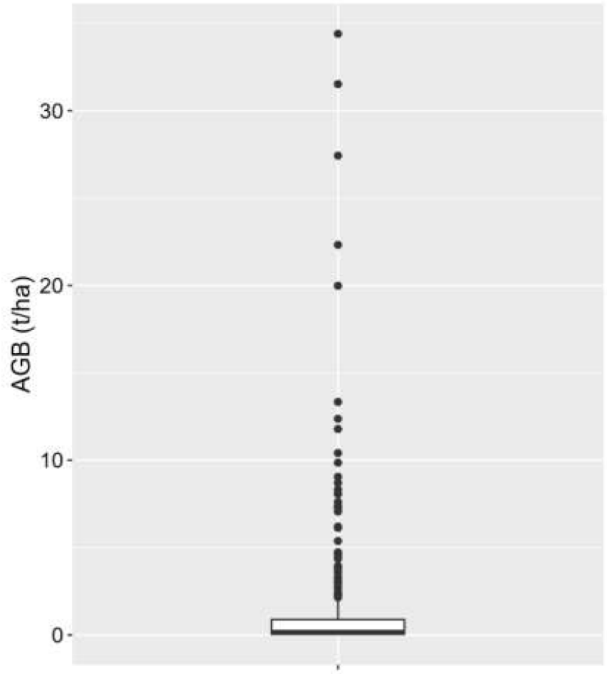

Fig. 6 Boxplot for field observed AGB

For the field calculated AGB, the highest correlation was obtained for the cross polarized bands from both sensors. Among them, the HV band of ALOS PALSAR-2 had the maximum correlation coefficient (R^2) of 0.16, and thereafter, VH band of Sentinel-1 had R^2 value 0.11. The ratio band from ALOS PALSAR-2 and the VV polarization of Sentinel-1 showed a similar relationship, giving a value of 0.08 for the correlation coefficient. Perhaps the R^2 values were lower for the polarimetric decomposition parameter from Sentinel-1, with the R^2 values less than 0.01. The correlation of various attributes with field observed AGB is shown in Fig. 7.

Table 1 Validation matrix for three models

Validation matrix	M1	M2	M3
R^2	0.64	0.44	0.62
RMSE	2.33	1.89	2.49
MAE	1.76	1.56	1.99

On validating the different models generated, it was found that the R^2 values for all the models ranged between 0.44 and 0.64, and the RMSE and MAE were between 1.89 t/ha and 2.49 t/ha and 1.56 t/ha and 1.99 t/ha, respectively. The highest R^2 value (0.64) was given by M1, which used Sentinel-1 variables, with RMSE 2.33 t/ha and MAE 1.76 t/ha. The lowest R^2 (0.44) value was given by M2, in which the ALOS PALSAR-2 variables were used. All three models gave adequate performance in the estimation of AGB. The R^2, RMSE, and MAE values for the models is given in Table 1. Though the highest R^2 value is given by M1, the least RMSE and MAE were given by M2. Fig. 8 displays the scatter plot of the models' predicted and observed AGB. After calculating the variable importance factor for each model, it was found that, for model M1, VV polarization contributed more than VH polarization. HV polarization was the most crucial parameter for M2, followed by HV/HH and HH polarization.

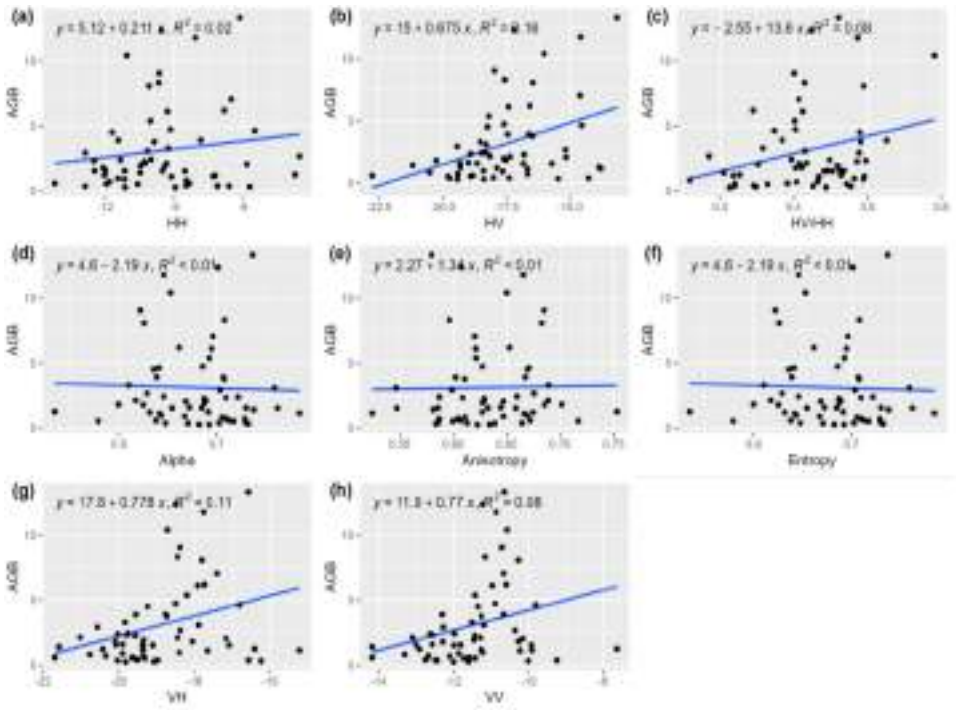

Fig. 7 Correlation of various attributes with field observed AGB; AGB vs (**a**) HH polarization (**b**) HV polarization (**c**) HV/HH of ALOS PALSAR-2 data (**d**) alpha (**e**) anisotropy (**f**) entropy (**g**) VH polarization and (**h**) VV polarization of Sentinel-1

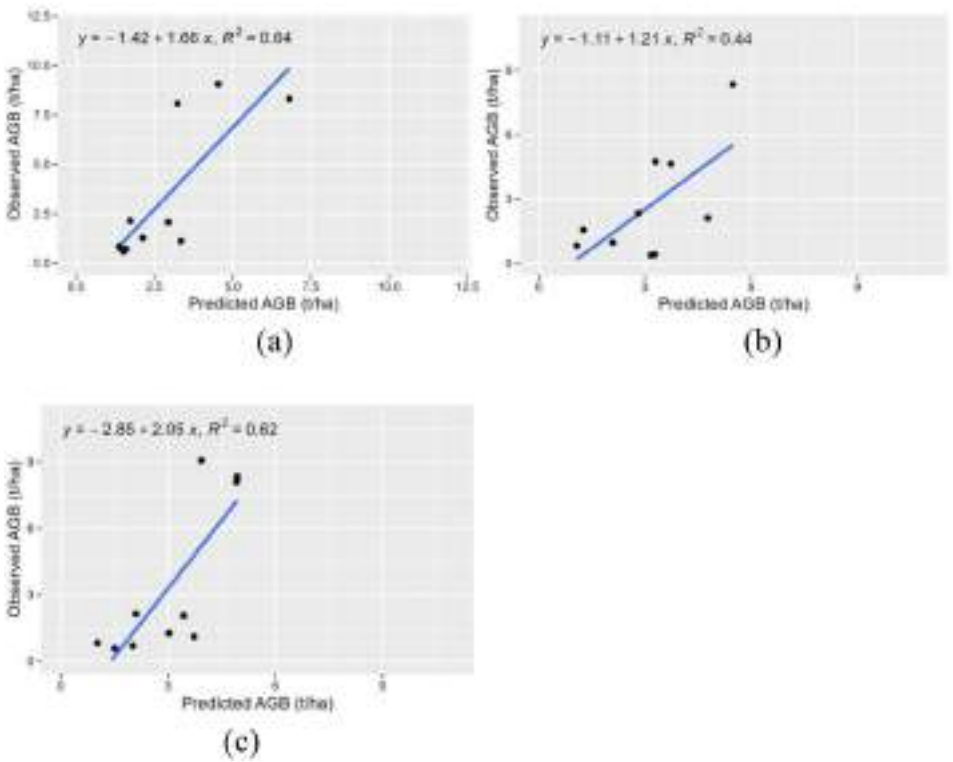

Fig. 8 Observed AGB vs predicted AGB scatter plot for (**a**) M1, (**b**) M2, (**c**) M3

Table 2 Distribution of AGB based on three models

AGB	M1	M2	M3
Low (< 3t/ha)	549.69	680.64	485.79
Medium (3–7 t/ha)	399.84	356.29	560.32
High (> 7t/ha)	132.07	52.41	41.35
Total	**1081.60**	**1089.35**	**1087.45**

Again, HV was the most important parameter in M3, followed by VV and VH polarizations, ratio band, HH polarization, and entropy. In M1 and M3, where polarimetric decomposition parameters were employed, it came as the least contributing factor. Above it, Sentinel-2 derived NDVI was used to mask out the water bodies, the built-up area, and the barren lands. The vegetation cover occupies an area of 1279 km^2 (49.44%) of the regional landscape. Then the AGB map for the vegetation cover of the entire study area was generated by extrapolating the model as the area shares similar physiography, mosaic land use, and climatic characteristics. The spatial distribution of AGB in the semi-arid regional landscape shows predominantly low biomass in the area (Table 2). The maps for AGB distribution in the study area based on different models are shown in Fig. 9.

4 Discussion

Biomass estimation of vegetation is very essential in semi-arid regions of India, as it is one among the largest climatic regions in India. The tree biomass outside forests received less attention as compared to forests. The interest and concern for estimating the biomass of ecosystems have been expanding over the past decades and remote sensing technology provides precise and transferable methodologies for this objective. While the potential of SAR data has been explored for AGB estimation, it was mostly in forested areas. In the present study in a semi-arid region, vegetation biomass was estimated using multi-frequency SAR data and the machine learning algorithm, random forest. The intention of the study was not only to estimate biomass but also to evaluate the performance of both Sentinel-1 (C-band) and ALOS PALSAR-2 (L-band) individually as well as synergistically in estimating the biomass of trees outside forest in semi-arid regions.

Studies have indicated a significant correlation between the variables of radar remote sensing and above-ground biomass, depending on the features of the vegetation canopy [44, 45]. It is obvious that the strength of the relationship varies strongly for forested areas and sparsely vegetated areas. The correlation of radar derived parameters in the current study showed a weak correlation to the field observed AGB; nonetheless, the cross-polarizations were having the highest correlation coefficient values. Different polarizations are sensitive to different scattering mechanisms, for instance, VV polarization is more sensitive to surface scattering due to water or bare soil, HH polarization is sensitive to double bounce scattering resulting from buildings and tree trunks, whereas the cross-polarizations VH and HV are more

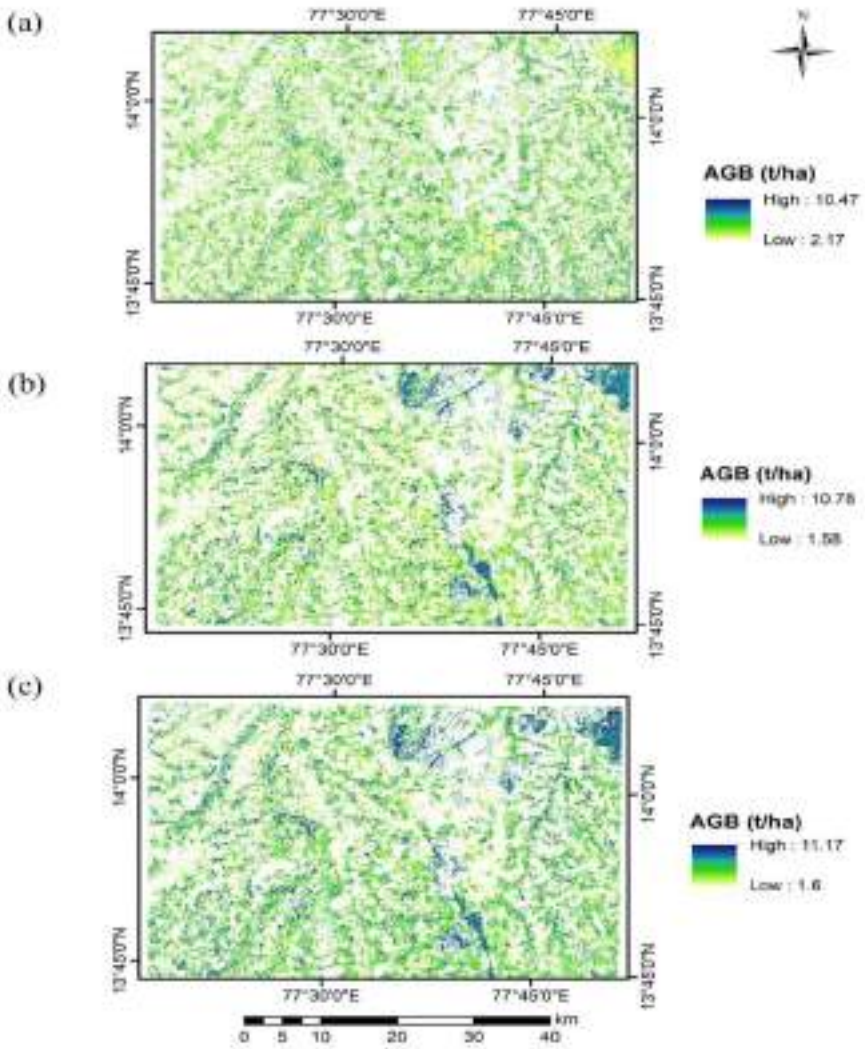

Fig. 9 Map of AGB distribution based on (**a**) M1, (**b**) M2 and (**c**) M3

sensitive to volume scattering from the foliage and branches of the tree canopy [44]. Specifically for biomass estimation, these cross-polarizations stand out due to their unique ability to capture the complex structural details within the vegetation stands, which are important in assessing AGB. The change in polarization from transmit to receive facilitates a more detailed identification of the complex interactions within forest canopies, enhancing the accuracy of AGB measurements. Moreover, VH and HV polarizations are more effective at mitigating the effects of surface characteristics, like soil moisture and texture, thereby providing a clearer and more direct assessment of AGB. This focus on the vegetative structure, rather than surface properties, enhances the efficacy of VH and HV polarizations in forest AGB estimation, ensuring more reliable results. The above findings have been confirmed by a number of previous studies [46–49] that have demonstrated comparable results. The findings of our study gave similar results to those in the pioneer studies. Roy et al., 2020 in their study found that the backscattering coefficient for VH polarization of Sentinel-1 had a higher correlation ($R^2 = 0.63$) than for the VV polarization ($R^2 = 0.44$) in the *Shorea robusta* dominated forest cover [10]. Similarly, Otukei and Emanuel, 2015, found a stronger correlation of AGB with the backscattering coefficient of HV polarization than with the HH polarization in the Bwindi Impenetrable National Park of Uganda [8]. Further, VH polarization was found to be more prominent than VV by Forkuor et al., 2020 [6]. The higher relationship of the cross polarized bands (VH and HV) indicates that they capture the structural information of the vegetation better than the co-polarized bands (VV and HH) [10].

Again, the Sentinel-1 image attributes produced by Dual-Polarimetric Decomposition displayed the least R^2 values. Jesus et al. (2023) employed the alpha angle and entropy derived from the Sentinel-1 dual-polarization decomposition technique to estimate the above-ground biomass (AGB) of arboreal Caatinga. Their findings indicated a limited correlation between the calculated alpha angle, entropy values,

and the AGB [28]. However, the combined use of the attributes provided better accuracy ($R^2 = 32.05\%$). Since, the pixels had a mixture of vegetation and bare soil, giving different scattering mechanisms, it is advantageous to explore the use of decomposition parameters.

A weak relationship was observed between the independent variables and field AGB in the study. This weaker correlation of the radar parameters can be due to the contribution of ground to the backscatter values since the impacts of soil factors such as soil roughness and moisture content in regions with sparse vegetation cover can affect the spectral responses, especially in semi-arid zones [3, 6, 50]. In addition, the SAR signal and plant canopy have a volumetric relationship, meaning that the amount of vegetation in a given pixel has a major impact on the SAR signal [13]. In the current study area, the vegetation is mostly scattered, so the exposure of soil has possibly affected the SAR signal.

The random forest models developed for biomass estimation using SAR data, gave acceptable performance, suggesting the potential of both L-band ALOS PALSAR-2 and C-band Sentinel-1 in estimating AGB in the selected semi-arid area. The results of our study agree with the previous studies, including the study by Jesus et al., 2023, where the attributes derived from Sentinel-1 were used for estimating the biomass of the Caatinga biome and found that the band ratio VH/VV, H, α,dual polarization synthetic aperture radar vegetation index (DPSVI) and cross-polarized VH for the intermediate period, and co-polarized VV for the green period were highly contributing to the regression model [28]. Wang et al., 2021 also found that the RADARSAT-2 C-band SAR data produced higher accuracy in stepwise multiple linear regression, in which the R^2 value ranged from 0.34 to 0.42 in the desert steppe [51]. Furthermore, the study noticed the underestimation of AGB in a few high biomass sites, suggesting the saturation of the model. Similar results were found by Bispo et al., 2020, in mapping the woody biomass of the Brazilian Savanna, with an underestimation of higher AGB levels and an overestimation of lower AGB levels [52]. The saturation of random forest modeling was observed in the study by Su et al., 2020, as well, with underestimation and overestimation of biomass in the subtropical forests in the northern Guangdong Province of China [36]. The range of predictions that random forest regression can generate is limited by the biggest and lowest values in the training set of data. As a result, estimates in the higher range may be underestimated, and those in the lower range may be overestimated [53]. Even though machine learning algorithms offer more effective means for establishing the complex non-linear relationships of remote sensing data with ecological features, they also come with certain associated problems, including the underestimation and overestimation of the data [54]. Remote sensing has proven to be a valuable tool for estimating biomass and productivity across local, regional, and global scales in recent times [55].

Our study highlighted the potential of SAR sensors operating at both C and L-bands are advantageous for estimating the spatial variation in AGB of vegetation outside the forest ecosystem. This study endeavoured to estimate the vegetation biomass across a regional scale with similar biogeographical, climatic, and agro-ecological conditions. The findings of the study are advantageous for understanding the dynamic changes in vegetation and promoting sustainable land management.

5 Conclusions

The estimation of the above ground biomass of trees has attracted a lot of attention in the scientific world; perhaps most of the studies concentrated on forest ecosystems. Our study evaluated the utility of two widely used SAR sensors, Sentinel-1 and ALOS PALSAR-2, in estimating AGB for semi-arid, the most predominate region. Three models were generated using the random forest algorithm, utilizing the data from the sensors solely and synergistically. R^2, RMSE, and MAE were used for validating the models, and they showed values ranging from 0.44 to 0.64 for R^2, from 1.89 t/ha to 2.49 t/ha for RMSE, and from 1.56 t/ha to 1.99 t/ha for MAE. The findings of the study demonstrate that the freely available versions of both sentinel-1 and ALOS PALSAR-2 data, individually and in combination, have immense potential for reliable biomass estimates in semi-arid regions with sparse vegetation cover, employing machine learning algorithms. Furthermore, the results of the study contribute valuable insights into AGB estimation methodologies, large area ecological plot, and emphasizing the significance of SAR remote sensing in monitoring biomass dynamics in challenging ecosystems in India's semi-arid regions, which in turn would provide valuable information for ecological restoration.

Acknowledgements We are thankful to the European Space Agency (ESA) for Sentinel-1 and Sentinel-2 data. We are grateful to JAXA and the Kyoto & Carbon Initiative for providing ALOS-2 PALSAR-2 data. Authors are grateful to the Shri G. Narayanaswamy, Pr. Additional Director General and Dr. K. Ezhilmathi, Additional Director, National Academy of Customs, Narcotics and Indirect Taxes (NACIN), Palasamudram, Andhra Pradesh, Director and Deputy Director (RSA), National Remote Sensing Centre, Hyderabad and Department of Environmental Sciences, All Saints' College, Thiruvananthapuram for the facilities, support and encouragement.

Author contributions Conceptualization and idea for the article: [A.S. Anjitha; C. Sudhakar Reddy]; Writing - original draft preparation and critical revision of the work: [A.S. Anjitha; N. Nitish Sri Surya; K.V. Satish; Smitha V. Asok; C. Sudhakar Reddy]; Visualization: [A.S. Anjitha]; Supervision: [C. Sudhakar Reddy; Smitha V. Asok].

Funding Not Applicable.

Data availability Not applicable.

Code availability Not applicable.

Declarations

Ethical approval This article does not contain any studies involving human/ animals performed by any of the authors.

Compliance with ethical standards Yes

Competing interests The authors declare no conflict of interest and have no known competing financial interests or personal relationships that could have appeared to influence the work reported in this article.

References

1. do Nascimento, D. M., Sales, A. T., Souza, R., da Silva, A. S. A., Sampaio, E. V. D. S. B., & Menezes, R. S. C. (2022). Development of a methodological approach to estimate vegetation biomass using remote sensing in the Brazilian semiarid NE region. *Remote Sensing Applications: Society and Environment*, 27, 100771. https://doi.org/10.1016/j.rsase.2022.100771.
2. Reddy, C. S., Satish, K. V., Saranya, K. R. L., Nitish Sri Surya, N., Neha, P. A., & Rajashekar, G. (2023). Harnessing essential biodiversity variables and remote sensing of earth observations - synthesizing biodiversity insights. *Spatial Information Research*. https://doi.org/10.1007/s41324-023-00558-6.
3. Eisfelder, C., Kuenzer, C., & Dech, S. (2011). Derivation of biomass information for semi-arid areas using remote-sensing data. *International Journal of Remote Sensing*, *33*, 2937–2984. https://doi.org/10.1080/01431161.2011.620034.
4. Eisfelder, C., Klein, I., Bekkuliyeva, A., Kuenzer, C., Buchroithner, M. F., & Dech, S. (2017). Above-ground biomass estimation based on NPP time-series–A novel approach for biomass estimation in semi-arid Kazakhstan. *Ecological Indicators*, *72*, 13–22. https://doi.org/10.1016/j.ecolind.2016.07.042.
5. Vafaei, S., Soosani, J., Adeli, K., Fadaei, H., Naghavi, H., Pham, T., et al. (2018). Improving Accuracy Estimation of Forest Aboveground Biomass based on incorporation of ALOS-2 PALSAR-2 and Sentinel-2A imagery and machine learning: A case study of the Hyrcanian Forest Area (Iran). *Remote Sensing*, *10*, 172. https://doi.org/10.3390/rs10020172.
6. Forkuor, G., Benewinde Zoungrana, J. B., Dimobe, K., Ouattara, B., Vadrevu, K. P., & Tondoh, J. E. (2020). Above-ground biomass mapping in west African dryland forest using Sentinel-1 and 2 datasets - a case study. *Remote Sensing of Environment*, *236*, 111496. https://doi.org/10.1016/j.rse.2019.111496.
7. Galidaki, G., Zianis, D., Gitas, I., Radoglou, K., Karathanassi, V., Tsakiri–Strati, M., et al. (2016). Vegetation biomass estimation with remote sensing: Focus on forest and other wooded land over the Mediterranean ecosystem. *International Journal of Remote Sensing*, *38*, 1940–1966. https://doi.org/10.1080/01431161.2016.1266113.
8. Otukei, J. R., & Emanuel, M. (2015). Estimation and mapping of above ground biomass and carbon of Bwindi impenetrable National Park using ALOS PALSAR data. *South African Journal of Geomatics*, *4*, 1.
9. Chang, J., & Shoshany, M. (2016). Mediterranean shrublands biomass estimation using Sentinel-1 and Sentinel-2. *2016 IEEE International Geoscience and Remote Sensing Symposium (IGARSS). IEEE*.
10. Roy, S., Mudi, S., Das, P., Ghosh, S., Shit, P. K., Bhunia, G. S., & Kim, J. (2021). Estimating above Ground Biomass (AGB) and Tree density using Sentinel-1 Data. *Spatial Modeling in Forest Resources Management* (pp. 259–280). Springer, Cham. https://doi.org/10.1007/978-3-030-56542-8_11.
11. Sivasankar, T., Lone, J. M., Sarma, K. K., Qadir, A., & Raju, P. L. N. (2018). The potential of multi-frequency multipolarized ALOS-2/PALSAR-2 and Sentinel-1 SAR data for aboveground forest biomass estimation. *International Journal of Engineering and Technology*, *10*, 797–802. https://doi.org/10.21817/ijet/2018/v10i3/181003095.
12. Crabbe, R. A., Lamb, D. W., Edwards, C., Andersson, K., & Schneider, D. (2019). A preliminary investigation of the potential of Sentinel-1 Radar to Estimate pasture Biomass in a grazed, native pasture Landscape. *Remote Sensing*, *11*, 872. https://doi.org/10.3390/rs11070872.
13. Patel, P., Srivastava, H. S., Panigrahy, S., & Parihar, J. S. (2006). Comparative evaluation of the sensitivity of multi-polarized multi-frequency SAR backscatter to plant density. *International Journal of Remote Sensing*, *27*, 293–305. https://doi.org/10.1080/01431160500214050.
14. Santos, J. R., Lacruz, M. S., Araujo, L. S., & Keil, M. (2002). Savanna and tropical rainforest biomass estimation and spatialization using JERS-1 data. *International Journal of Remote Sensing*, *23*, 1217–1229. https://doi.org/10.1080/01431160110092867.
15. Carreiras, J., Melo, J., & Vasconcelos, M. (2013). Estimating the Above-Ground Biomass in Miombo Savanna Woodlands (Mozambique, East Africa) using L-Band Synthetic aperture Radar Data. *Remote Sensing*, *5*, 1524–1548. https://doi.org/10.3390/rs5041524.
16. Tanase, M. A., Panciera, R., Lowell, K., Tian, S., Garcia-Martin, A., & Walker, J. P. (2014). Sensitivity of L-Band Radar Backscatter to Forest Biomass in Semiarid environments: A comparative analysis of Parametric and Nonparametric models. *IEEE Transactions on Geoscience and Remote Sensing*, *52*, 4671–4685. https://doi.org/10.1109/TGRS.2013.2283521.
17. Mermoz, S., Le Toan, T., Villard, L., Réjou-Méchain, M., & Seifert-Granzin, J. (2014). Biomass assessment in the Cameroon savanna using ALOS PALSAR data. *Remote Sensing of Environment*, *155*, 109–119. https://doi.org/10.1016/j.rse.2014.01.029.
18. Behera, M. D., Tripathi, P., Mishra, B., Kumar, S., Chitale, V. S., & Behera, S. K. (2016). Above-ground biomass and carbon estimates of Shorea robusta and Tectona grandis forests using QuadPOL ALOS PALSAR data. *Advances in Space Research*, *57*, 552–561. https://doi.org/10.1016/j.asr.2015.11.010.
19. Thumaty, K. C., Fararoda, R., Middinti, S., Gopalakrishnan, R., Jha, C. S., & Dadhwal, V. K. (2015). Estimation of Above Ground Biomass for Central Indian deciduous forests using ALOS PALSAR L-Band Data. *Journal of the Indian Society of Remote Sensing*, *44*, 31–39. https://doi.org/10.1007/s12524-015-0462-4.
20. Bouvet, A., Mermoz, S., Le Toan, T., Villard, L., Mathieu, R., Naidoo, L., & Asner, G. P. (2018). An above-ground biomass map of African savannahs and woodlands at 25 m resolution derived from ALOS PALSAR. *Remote Sensing of Environment*, *206*, 156–173. https://doi.org/10.1016/j.rse.2017.12.030.
21. Chang, Q., Zwieback, S., DeVries, B., & Berg, A. (2022). Application of L-band SAR for mapping tundra shrub biomass, leaf area index, and rainfall interception. *Remote Sensing of Environment*, *268*, 112747. https://doi.org/10.1016/j.rse.2021.112747.
22. Velasco Pereira, E. A., Varo Martínez, M. A., Ruiz Gómez, F. J., & Navarro-Cerrillo, R. M. (2023). Temporal changes in Mediterranean Pine Forest Biomass using synergy models of ALOS PALSAR-Sentinel 1-Landsat 8 sensors. *Remote Sensing*, *15*, 3430. https://doi.org/10.3390/rs15133430.

23. Periasamy, S. (2018). Significance of dual polarimetric synthetic aperture radar in biomass retrieval: An attempt on Sentinel-1. *Remote Sensing of Environment*, *217*, 537–549. https://doi.org/10.1016/j.rse.2018.09.003.
24. Bao, N., Li, W., Gu, X., & Liu, Y. (2019). Biomass Estimation for Semiarid Vegetation and Mine Rehabilitation using Worldview-3 and Sentinel-1 SAR Imagery. *Remote Sensing*, *11*, 2855. https://doi.org/10.3390/rs11232855.
25. Cartus, O., Santoro, M., Wegmuller, U., Labriere, N., & Chave, J. (2022). Sentinel-1 coherence for Mapping above-ground Biomass in Semiarid Forest Areas. *IEEE Geoscience and Remote Sensing Letters*, *19*, 1–5. https://doi.org/10.1109/LGRS.2021.3071949.
26. Dave, R. B., Saha, K., Kushwaha, A., Vithalpura, M., Nidhin, P., & Murugesan, A. (2023). Analysing the potential of polarimetric decomposition parameters of Sentinel–1 dual-pol SAR data for estimation of rice crop biophysical parameters. *Journal of Agrometeorology*, 25. https://doi.org/10.54386/jam.v25i1.2039.
27. De Petris, S., Sarvia, F., Gullino, M., Tarantino, E., & Borgogno-Mondino, E. (2021). Sentinel-1 polarimetry to Map Apple Orchard damage after a storm. *Remote Sensing*, *13*, 1030. https://doi.org/10.3390/rs13051030.
28. Jesus, J. B., Kuplich, T. M., Barreto, Í. D., & Gama, D. C. (2023). Dual polarimetric decomposition in Sentinel-1 images to estimate aboveground biomass of arboreal caatinga. *Remote Sensing Applications: Society and Environment*, *29*, 100897. https://doi.org/10.1016/j.rsase.2022.100897.
29. Schlund, M., & Davidson, M. W. J. (2018). Aboveground Forest Biomass Estimation combining L- and P-Band SAR Acquisitions. *Remote Sensing*, *10*, 1151. https://doi.org/10.3390/rs10071151.
30. Berninger, A., Lohberger, S., Stängel, M., & Siegert, F. (2018). SAR-Based estimation of above-ground biomass and its changes in tropical forests of Kalimantan using L- and C-Band. *Remote Sensing*, *10*, 831. https://doi.org/10.3390/rs10060831.
31. Naidoo, L., Mathieu, R., Main, R., Kleynhans, W., Wessels, K., Asner, G., et al. (2015). Savannah woody structure modelling and mapping using multi-frequency (X-, C- and L-band) synthetic aperture radar data. *ISPRS Journal of Photogrammetry and Remote Sensing*, *105*, 234–250. https://doi.org/10.1016/j.isprsjprs.2015.04.007.
32. Behera, D., Kumar, V. A., Rao, J. P., Padal, S. B., Ayyappan, N., & Reddy, C. S. (2023). Estimating aboveground biomass of a regional forest landscape by integrating textural and spectral variables of Sentinel-2 along with ancillary data. *Journal of Indian Society of Remote Sensing*. https://doi.org/10.1007/s12524-023-01740-x.
33. Ayushi, K., Babu, K. N., Ayyappan, N., Nair, J. R., Athira, K., & Reddy, C. S. (2024). A comparative analysis of machine learning techniques for aboveground biomass estimation: A case study of the western ghats, India. *Ecological Informatics*.https://doi.org/10.1016/j.ecoinf.2024.102479.
34. Arachchige, C. M., Nashrrullah, S., Gunasekara, K., & Hazarika, M. K. (n.d.). Estimation of Forest above-ground Biomass using Random Forest Algorithm based on ALOS PALSAR and Landsat 5TM Imageries.
35. Tuong, T. T. C., Tani, H., Wang, X., Thang, N. Q., & Bui, H. M. (2020). Combination of SAR Polarimetric Parameters for Estimating Tropical Forest Aboveground Biomass. *Polish Journal of Environmental Studies*, *29*, 3353–3365. https://doi.org/10.15244/pjoes/112900.
36. Su, H., Shen, W., Wang, J., Ali, A., & Li, M. (2020). Machine learning and geostatistical approaches for estimating aboveground biomass in Chinese subtropical forests. *Forest Ecosystems*, *7*(64). https://doi.org/10.1186/s40663-020-00276-7
37. Purohit, S., Aggarwal, S. P., & Patel, N. R. (2021). Estimation of forest aboveground biomass using combination of Landsat 8 and Sentinel-1A data with random forest regression algorithm in Himalayan Foothills. *Tropical Ecology*, *62*, 288–300. https://doi.org/10.1007/s42965-021-00140-x.
38. Reddy, C. S., & Satish, K. V. (2024). Assessment of tree density, tree cover, species diversity and biomass in semi-arid human dominated landscape using large-area inventory and remote sensing data. *Anthropocene Science*.https://doi.org/10.1007/s44177-024-00066-8.
39. Chave, J., Réjou-Méchain, M., Búrquez, A., Chidumayo, E., Colgan, M. S., Delitti, W. B., et al. (2014). Improved allometric models to estimate the aboveground biomass of tropical trees. *Global Change Biology*, *20*, 3177–3190. https://doi.org/10.1111/gcb.12629.
40. Cloude, S. (2007). The dual polarization entropy/alpha decomposition: A PALSAR case study. *Proceedings of the 3rd International Workshop on Science and Applications of SAR Polarimetry and Polarimetric Interferometry* (Vol. 644, p. 2).
41. Shan, Z., Wang, C., Zhang, H., & Chen, J. (2011). & others. H-alpha decomposition and alternative parameters for dual Polarization SAR data. Proc. PIERS, Suzhou, China.
42. Rouse Jr, J. W., Haas, R. H., Deering, D. W., Schell, J. A., & Harlan, J. C. (1974). *Monitoring the vernal advancement and retrogradation (green wave effect) of natural vegetation*. Tech. rep.
43. Breiman, L. (2001). Random Forests. *Machine Learning*, 45, 5–32. https://doi.org/10.1023/A:1010933404324.
44. Meyer, F. (2019). Spaceborne Synthetic Aperture Radar: Principles, Data Access, and Basic Processing Techniques. *The SAR Handbook. Comprehensive Methodologies for Forest Monitoring and Biomass Estimation* (1st ed., pp. 21–43). Huntsville, AL, USA. https://doi.org/10.25966/nr2c-s697.
45. Sainuddin, F. V., Malek, G., Rajwadi, A., Nagar, P. S., Asok, S. V., & Reddy, C. S. (2024). Estimating above-ground biomass of the Regional Forest Landscape of Northern Western Ghats using machine learning algorithms and Multi-sensor Remote Sensing Data. *Journal of the Indian Society of Remote Sensing*, https://doi.org/10.1007/s12524-024-01836-y.
46. Dobson, M. C., Ulaby, F. T., Pierce, L. E., Sharick, T. L., Bergen, K. M., Kellndorfer, J., Kendra, J. R., Li, E., Lin, Y. C., Nashashbi, A., Sarabandi, K., & Siqueira, P. (1995). Estimation of forest biophysical characteristics in Northern Michigan with SIRC/X-SAR. *IEEE Transactions on Geoscience and Remote Sensing*, *33*(4), 877–895. https://doi.org/10.1109/36.406674.
47. Ranson, K. J., & Sun, G. (1994). Mapping biomass of a Northern forest using multifrequency SAR data. *IEEE Transactions on Geoscience and Remote Sensing*, *32*(2), 388–396.
48. Mitchard, E. T. A., Saatchi, S. S., Lewis, S. L., Feldpausch, T. R., Woodhouse, I. H., Sonké, B., Rowland, C., & Meir, P. (2011). Measuring biomass changes due to woody encroachment and deforestation/degradation in a forest-savanna boundary region of Central Africa using multi-temporal L-band radar backscatter. *Remote Sensing of Environment*, *115*(11), 2861–2873. https://doi.org/10.1016/j.rse.2010.02.022.
49. Sainuddin, F. V., Chirakkal, S., Asok, V. S., Das, K. A., & Putrevu, D. (2023). Evaluation of Multifrequency SAR Data for Estimating Tropical Above-Ground Biomass by Employing Radiative Transfer Modeling. *Environmental Monitoring and Assessment*, 195(9), 1102. https://doi.org/10.1007/s10661-023-11715-7
50. Ghosh, S. M., & Behera, M. D. (2018). Aboveground biomass estimation using multi-sensor data synergy and machine learning algorithms in a dense tropical forest. *Applied Geography*, *96*, 29–40. https://doi.org/10.1016/j.apgeog.2018.05.011.
51. Wang, X. Y., Pan, P. P., & Lu, J. (2021). Estimation of shrubland aboveground biomass of the desert steppe from optical and C-band SAR data. *Geocarto International*, *37*, 4509–4526. https://doi.org/10.1080/10106049.2021.1886346.
52. Bispo, P., Rodríguez-Veiga, P., Zimbres, B., do, Couto de Miranda, S., Henrique Giusti Cezare, C., Fleming, S. (2020).

Woody Aboveground Biomass Mapping of the Brazilian Savanna with a Multi-Sensor and Machine Learning Approach. *Remote Sensing*, 12, 2685.
53. Nunes, M. H., & Görgens, E. B. (2016). Artificial Intelligence Procedures for Tree Taper Estimation within a Complex Vegetation Mosaic in Brazil. *PloS one*, 11, e0154738. https://doi.org/10.1371/journal.pone.0154738.
54. Malhi, R. K., Anand, A., Srivastava, P. K., Chaudhary, S. K., Pandey, M. K., Behera, M. D., & Kiran, G. S. (2022). Synergistic evaluation of Sentinel 1 and 2 for biomass estimation in a tropical forest of India. *Advances in Space Research*, *69*, 1752–1767. https://doi.org/10.1016/j.asr.2021.03.035.
55. Reddy, C. S., Rakesh, F., Jha, C. S., Athira, K., Singh, S., Alekhya, V. V. L. P., Rajashekar, G., Diwakar, P. G., & Dadhwal, V. K. (2016). Geospatial assessment of long-term changes in carbon stocks and fluxes in forests of India (1930–2013). *Global and Planetary Change*, *143*, 50–65. https://doi.org/10.1016/j.gloplacha.2016.05.011.
56. Gorelick, N., Hancher, M., Dixon, M., Ilyushchenko, S., Thau, D., & Moore, R. (2017). Google earth engine: Planetary-scale geospatial analysis for everyone. *Remote sensing of Environment*, 202, 18–27. https://code.earthengine.google.com/.
57. Hijmans, R. J. (2023). Terra: Spatial Data Analysis. R package version 1.7-39. The R Foundation for Statistical Computing. https://cran.r-project.org/package=terra.
58. R Core Team. (2023). R: A Language and Environment for Statistical Computing. R Foundation for Statistical Computing, Vienna, Austria. https://www.R-project.org/.
59. https://dataspace.copernicus.eu/.
60. https://step.esa.int/main/download/snap-download/.
61. Liaw, A., & Wiener, M. (2002). Classification and regression by randomForest. R News 2(3), 18–22. https://cran.r-project.org/package=randomForest.